THREE-DIMENSIONAL IMAGE OF THE HUMAN TOOTH BASED ON OPTICAL COHERENCE TOMOGRAPHY

Y. Liang, X. S. Yao, and S. Lan

Key Laboratory of Opto-electronics Information
and Technical Science of MOE
College of Precision Instrument & Opto-electronics Engineering
Tianjin University
Tianjin 300072, China

H. Yao

Research Center at Tianjin Stomatological Hospital
Tianjin 300041, China

T. Liu, M. Wan, and Y. Liang

Key Laboratory of Opto-electronics Information
and Technical Science of MOE
College of Precision Instrument & Opto-electronics Engineering
Tianjin University
Tianjin 300072, China

Y. Li

Research Center at Tianjin Stomatological Hospital
Tianjin 300041, China

B. Shi

Key Laboratory of Opto-electronics Information
and Technical Science of MOE
College of Precision Instrument & Opto-electronics Engineering
Tianjin University
Tianjin 300072, China

G. Wang

Research Center at Tianjin Stomatological Hospital
Tianjin 300041, China

Corresponding author: Y. Liang (liangyan1120_0@yahoo.com.cn).

Abstract—A method of acquiring clear three-dimensional image of human tooth in vitro, which is based on optical coherence tomography, is described. The background noise of the cross-section image is eliminated by image preprocessing algorithms, then the three-dimensional image is reconstructed by ray-casting algorithm and gives the whole view of dental crown which contains dentin and enamel. A plane can be used to cut the tooth interactively to observe the inner tissue. This image is convenient for doctors to locate lesions and has a great potential for the clinical diagnosis of early dental caries.

1. INTRODUCTION

Dental health is an important part of human health. Traditionally, dentists evaluate the oral health of a patient through three main methods: visual/tactile examination, periodontal probing, and radiographic imaging. The method of the probes can be painful, and the diagnosis is influenced by variations on insertion force, inflammatory statues of tissue, diameter of probe tips, and anatomical tooth contours. Radiographies have several limitations in identifying periodontal diseases as they provide no information about soft issue. Also they are two dimensional, and finding the precise position of a caries lesion is very difficult or even impossible and harmful to patients [1, 2]. Optical coherence tomography (OCT) has attracted extensive research as a non-contact high resolution technique for obtaining cross-section images of the internal microstructure of living tissues. Since Huang et al. [3] obtained the first OCT image of the tiny structure of human retina in 1991, many research groups have obtained clear OCT images of both normal and decayed dental tissues [4–8, 18, 19] and proved its usefulness in diagnosis.

But the dental images of those researches [4–8, 18] are basically two-dimensional, which is called B-scan (tomograms). These B-scans are obtained at sites presumptively chosen during the examinations. Obviously, more comprehensive information is desirable if we want to detect disease at early stage or monitor response to therapy in clinical practice. The ability to acquire three-dimensional or volumetric information is attractive because it can provide complete structural information [20]. The three-dimensional image in [1] is just the dental microstructure, which is inconvenient in clinical practice, because doctors need to locate lesions from the whole view of the teeth. Another different application is the three-dimensional recording in biological tissues for personal identification [21].

The goal of this work is to acquire three-dimensional image

of human tooth based on all-fiber OCT system. It contains more comprehensive structure information than the cross-section image and is convenient for doctors to locate lesions exactly. It gives the whole view of dental crown and enamel, and dentin can be seen clearly. The three-dimensional image is reconstructed by ray-casting algorithm. Ray-casting is a volume rendering method, which omits the intermediate geometric representation and involves direct projection of the entire 3D dataset onto a 2D display [14]. The image preprocessing methods are chosen to eliminate the background noise of the cross-section image. A cutting plane is interactively used to cut the tooth tissue for observing the inner structure.

2. THE ALL-FIBER OCT SYSTEM

The OCT system utilizes the principle of low-coherence interferometry with a broadband light source for obtaining high special resolution [9]. According to the basic theory of OCT and to overcome the polarization sensitivity commonly found in all-fiber OCT systems, a polarization insensitive scheme was adopted. Fig. 1 shows the schematic diagram of all-fiber polarization insensitive OCT system.
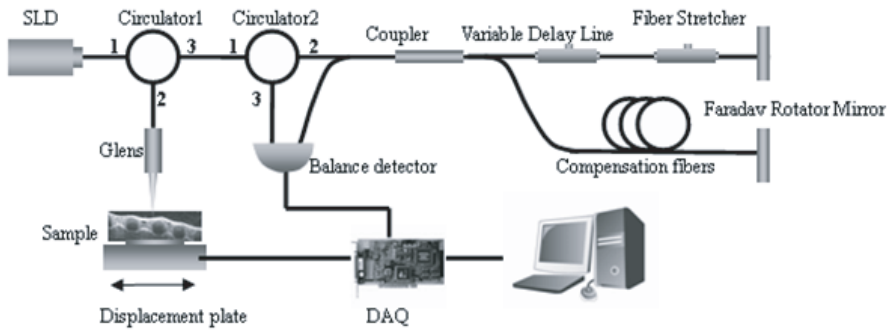

Figure 1. Schematic of the all-fiber OCT system.

The system uses a SLD with a FWHM bandwidth of 50 nm and a center wavelength of 1310 nm as a light source, resulting in a free-space coherence length of 15 μm. Teeth are high scattering tissue; the attenuation of light inside the teeth is primarily from scattering; and the absorption is negligible. Near-infrared light at 1310 nm waveband has the maximum penetration depth and is well suited for the detection and imaging of interproximal caries lesions [10, 11]. Light is delivered to the sample by a GRIN lens with a focal length of 3 mm. The reflected light from the exiting surface of GRIN lens is used as the reference

signal. One arm of the interferometer consists of a fiber stretcher based on scanning optical delay line with 3 mm delay range and a variable delay line (VDL) for matching the optical length between the two interferometer arms. A Faraday rotator mirror is placed at each end of the interferometer arms for eliminating polarization fluctuations in the single mode fiber. Note that such an arrangement completely eliminates polarization sensitivity, even when the sample arm and the interferometer arms are perturbed. The balanced detector receives the interference signal, and it can eliminate the common mode noises and the DC signal. The DAQ card collects the data to the computer. A two-dimensional displacement stage driven by the stepper motor is used for the transverse scans of the sample.

3. THE CROSS-SECTION IMAGE OF HUMAN TOOTH

The tooth was kept in distilled water and was fixed on the two-dimensional displacement stage. Fig. 2 shows the three-dimensional scan directions. Z direction is the depth scan (A-scan), and X is the transverse scan direction; adding another Y we can generate the three-dimensional image. The OCT cross-section images are constructed along X and Z directions.
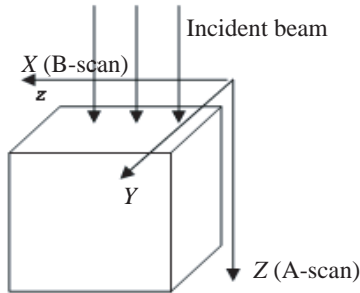
Figure 2. The three-dimensional scanning directions. Z is produced by the optical length scan of the system. X and Y are the transverse scan directions.

The raw interference data were smoothed by the band-pass filter. The parameter of the filter was determined by the driver frequency of fiber stretcher, f_s. The maximum optical length change of fiber stretcher is l_m (in the air). Then the carrier wave frequency of the interference signal is
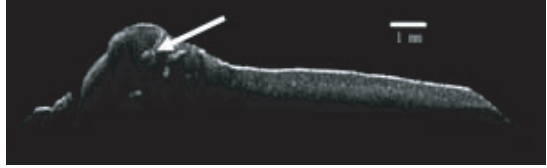
$$f = \frac{4 f_s l_m}{\lambda_0} \tag{1}$$

where λ_0 is the center wave length of broadband light source. The interference signal bandwidth is [12]

$$\Delta f = \frac{\Delta \lambda}{\lambda_0} f \tag{2}$$

where $\Delta \lambda$ is the bandwidth of the light source. We extracted the interference signal envelope based on Hilbert transformation.

**Figure 3.** The human tooth in vitro.

Figure 4. The OCT cross-section image of the tooth. There are some cracks in the crown indicated by the arrow.

Figure 3 shows a human tooth in vitro used in the experiment. Its OCT cross-section image is shown in Fig. 4. All scans were normalized to a maximum OCT signal, and a false-color gray scale was used. We can see clearly that there are some cracks in the crown.

4. 3D IMAGE RECONSTRUCTION OF THE HUMAN TOOTH

Volume visualization is realized by projecting a three-dimensional dataset onto a two-dimensional image plane, so we can gain an understanding of the structure contained within the data volume. The data volume is usually treated as an array of volume elements (voxels), as shown in Fig. 5. Each voxel has 8 grid-points. The values of the dataset are distributed on the 8 grid-points of the voxels. The fundamental volume visualization algorithms fall into two categories, direct volume rendering (DVR) algorithms and surface-fitting (SF) algorithms. Ray-casting belongs to DVR, while marching cubes belong to SF. DVR methods are characterized by mapping elements directly into screen space without using geometric primitives as an intermediate representation. SF algorithms typically fit surface primitives such as polygons or patches to constant-value contour surfaces in volumetric datasets. The user begins by choosing a threshold value, and then geometric primitives are automatically fit to the high-contrast contours in the volume that match the threshold. Cells whose values are all
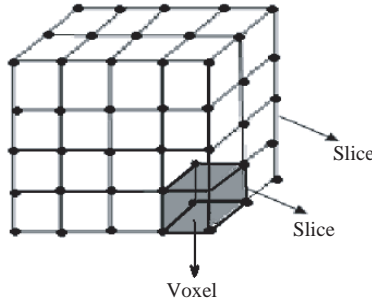
Figure 5. Data volume.

above the chosen threshold or all below the threshold are discarded and have no effect on the final image. Showing just the cells falling on the threshold is sometimes useful, but can be a problem. Another consideration is the huge number of surface primitives generated for large volumetric datasets. Ray-casting is chosen since it makes full use of the entire 3D dataset. It has much higher image quality and can give more details of the structure [14]. Ray-casting conducts an image-order traversal of the image plane pixels, finding a color and opacity for each [13, 15]. The procedure is shown in Fig. 6 [16].

The first step is the dataset acquisition. In our experiment, 97 OCT cross-section (slice) images of the sample were obtained. The size of the cross-section image is 455×291. Fig. 7 shows four image examples and the sample. The cross-section image is made up of the dental crown, which contains enamel and dentin.

The next step is the data preprocessing. Since there is much noise in the background of the original cross-section images gained in the experiment the gray scale of it even can compare with the dentin, which will make identifying the edge of tooth difficult and therefore will influence the result of the reconstruction. The method is that we should extract the contour of the tooth tissue. First, we use the median filter to reduce the impulse noise. Then we improve the contrast of the image through histogram equalization. And the image binarization can remove the noise that has lower gray value. After that, edge extracting is done based on Sobel-operator. However, some of the extracted contours are broken. The broken contours are connected through mathematical morphology. Finally, we extract the biggest contour based on connect domain which is the contour of the tooth tissue. Fig. 8(a) shows the original image; (b) shows the histogram equalization result; and (c) shows its contour.

With the position of the background is determined, we can assign
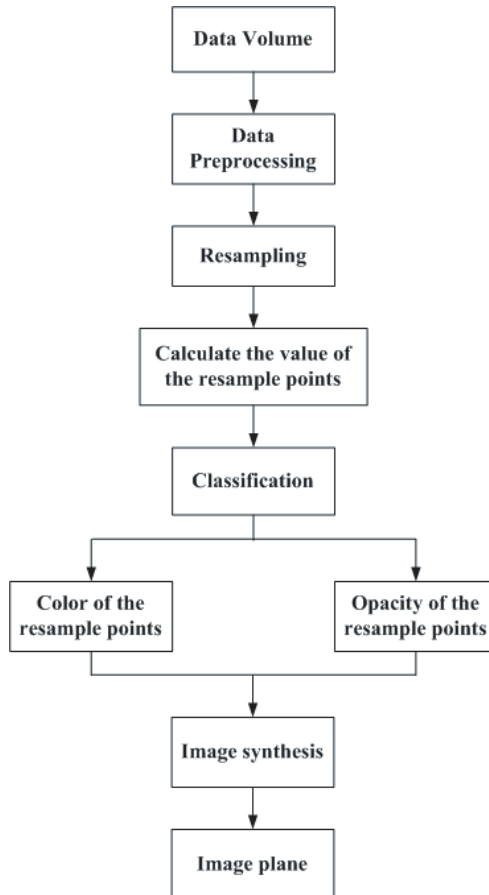
Figure 6. The procedure of the ray-casting algorithm.

zero to it to make the background black. Repeating the procedures until all slices are processed.

Then we put the data slices into an array of voxels as mentioned before. These voxels comprise the 3D dataset. After that a ray is launched from each pixel of the image plane through the data volume along our observation direction. Along each ray, a certain amount of resample points are chosen, which are equally spaced. This step is called resampling, as shown in Fig. 9.

In our method there are two coordinates; one represents the volume data called object coordinate; the other represents the image plane called image coordinate. The resample points are described in the image coordinate. In order to find the values of the resample

points, we should transform them from the image coordinate to object coordinate. Fig. 10 shows the transform between two coordinates. XYZ represents the image coordinate, and UVW represents the object coordinate. The observation direction is determined by the user. So we can assume that UVW is obtained from XYZ by rotating it around a zeroaxial axis k with an angle θ, and k is a unit vector. The equation

(a)

(b)
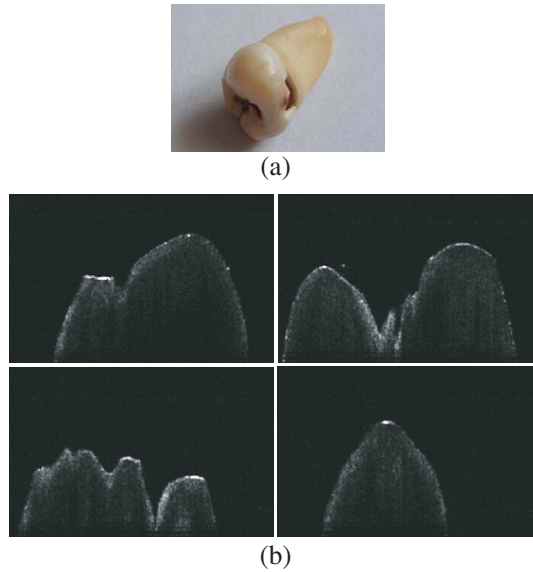
Figure 7. (a) The sample for three-dimensional reconstruction, (b) four cross-section images.

(a)   (b)   (c)
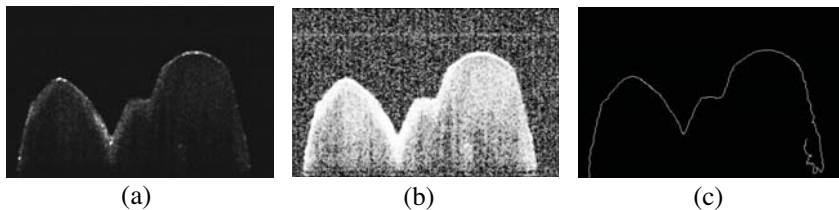
Figure 8. The crown image and its contour. (a) The original image, (b) The histogram equalization result, (c) the contour of it.

is referred as (3). $k = \sqrt{k_x^2 + k_y^2 + k_z^2}$. (x, y, z) is the point before rotating, and (x', y', z') is the point after rotating.

$$
\begin{bmatrix} x' \\ y' \\ z' \end{bmatrix} = \begin{bmatrix} k_x k_x (1-\cos\theta) + \cos\theta & k_y k_x (1-\cos\theta) - k_z \sin\theta \\ k_x k_y (1-\cos\theta) + k_z \sin\theta & k_y k_y (1-\cos\theta) + \cos\theta \\ k_x k_z (1-\cos\theta) - k_y \sin\theta & k_y k_z (1-\cos\theta) + k_x \sin\theta \end{bmatrix}
$$
$$
\begin{matrix} k_z k_x (1-\cos\theta) + k_y \sin\theta \\ k_z k_y (1-\cos\theta) - k_x \sin\theta \\ k_z k_z (1-\cos\theta) + \cos\theta \end{matrix} \begin{bmatrix} x \\ y \\ z \end{bmatrix} \qquad (3)
$$

Thus we can know the three axial vector coordinates of UVW in XYZ.

To find the value of the resample point, an interpolation is performed by the closest eight grid-points. Then according to the
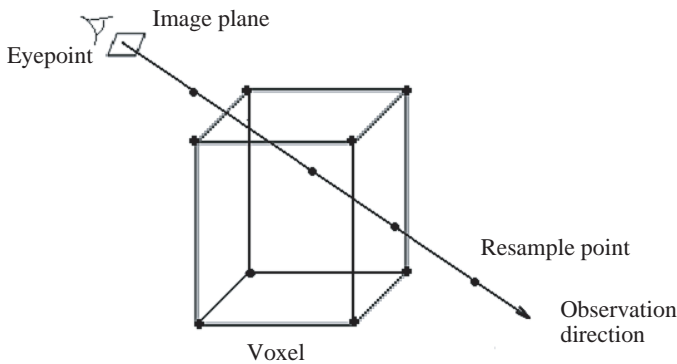

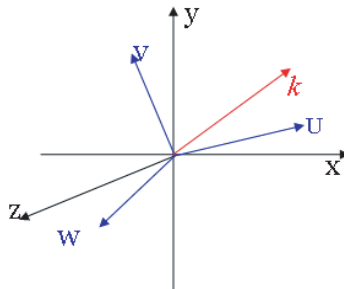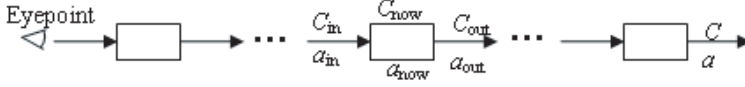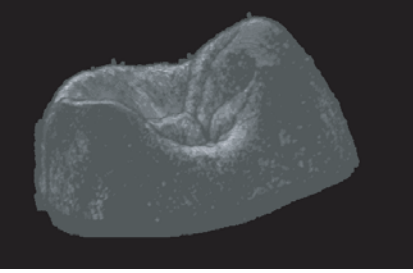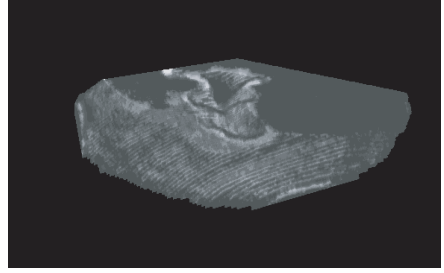**Figure 9.** The principle of resampling.

Figure 10. The image and object coordinates.

Figure 11. The front-to-back image synthesis.

Figure 12. Three-dimensional image of the sample.

Figure 13. The inner structure of tooth.

value, we should classify the point, which means choosing color (brightness) and opacity (light attenuation) values to go with each possible range of data values. The range of opacity is 0 to 1. Since the tissue in the cross-section image can be divided into two parts, enamel and dentin, there are two ranges of the resample points. One represents the enamel; the other represents the dentin.

The last step is the front-to-back image synthesis. The opacities and colors of the resample points encountered along the ray are summed to find the opacity and color of the pixel. Fig. 11 shows the image synthesis [17] with C represents the color of the resample point, and a represents the opacity of the resample point. And the equation is referred as (4).

$$C_{out}a_{out} = C_{in}a_{in} + C_{now}a_{now}(1 - a_{in})$$
$$a_{out} = a_{in} + a_{now}(1 - a_{in})$$

$$(4)$$

The front-to-back traversal is chosen, because the resample points in the back do not have to be traversed if the resample points in the front have already created a complete image. This means that the opacity value will increase gradually. When it approaches 1, the pixel is near to be totally opaque. The subsequent resample points will not contribute to the image, and do not need to be calculated. This method avoids useless calculation and can be faster.

Each pixel of the image plane can be shown with its color and opacity. Then the three-dimensional image is reconstructed.

The result is shown in Fig. 12. It gives the whole view of dental crown. The brighter part represents the enamel, and the darker part is the dentin.

In order to observe the inner tissue interactively, a cutting plane determined by the mouse is used to cut the tooth. The resample points above the cutting plane need not to be calculated. The result is shown in Fig. 13. The middle of the image is enamel, which is brighter.

5. DISCUSSION AND CONCLUSION

We developed a method to acquire three-dimensional image of the human tooth in vitro based on all-fiber OCT system. The image was reconstructed by ray-casting algorithm. There are many advantages of the algorithm. The image shows the entire dataset, not just a collection of thin surfaces as in SF, and its quality is much higher. It can also show the details of the structure. Ray-casting can be parallelized at pixel level since rays from all the pixels in the image plane can be cast independently. The disadvantages of ray-casting are that it is slower than SF and the entire dataset must be traversed each time an image is rendered. In the experiment, three-dimensional image was reconstructed using 97 cross-section images. The size of the cross-section image is 455×291 pixels. The depth scan (A-scan) of the OCT system is 3 mm, and the transverse scan (B-scan) is 7.5 mm. So the cross-section images are large enough to observe the dental crown tissue. The three-dimensional image, Fig. 12, clearly shows the general view of dental crown, including enamel and dentin. It will be convenient for doctors to locate lesions exactly. Before reconstruction, we did the image processing to eliminate the background noise of the cross-section images. The front-to-back image synthesis can accelerate the calculation. We also provided an interactive function, i.e., a cutting plane can be used to cut the tooth tissue for observing the inner structure, as shown in Fig. 13. This method will be of great benefit to the clinical diagnosis of early dental caries.

ACKNOWLEDGMENT

REFERENCES

1. Freitas, A. Z., D. M. Zezell, and N. D. Vieira, Jr., "Imaging carious human dental tissue with optical coherence tomography," *Journal of Applied Physis*, Vol. 99, No. 024906, 1–6, 2006.

2. Mayfield, L., G. Bratthall, and R. Attstrom, "Periodontal probe precision using four different periodontal probes," *J. Clin. Periodontology*, Vol. 23, No. 76, 76–82, 1996.

3. Huang, D., C. P. Swanson, J. S. Lin, et al., "Optical coherence tomography," *Science*, Vol. 254, No. 5035, 178–1181, 1991.

4. Colston, B. W., M. J. Everett, U. S. Sathyam, et al., "Imaging of the oral cavity using optical coherence tomography," *Monogr. Oral Sci.*, Vol. 17, 32–55, 2000.

5. Baumgartner, A., S. Dichtl, C. K. Hitzenberger, et al., "Polarization-sensitive optical coherence tomography of dental structures," *Caries Res.*, Vol. 34, No. 1, 59–69, 2000.

6. Amaechi, B. T., S. M. Higham, A. G. Podoleanu, et al., "Use of optical coherence tomography for assessment of dental caries: Quantitative procedure," *J. Oral Rehabil.*, Vol. 28, No. 12, 1092–1093, 2001.

7. Closton, B. W., Jr., M. J. Everett, et al., "Imaging of hard- and soft-tissue structure in the oral cavity by optical coherence tomography," *Applied Optics*, Vol. 37, No. 16, 3582–3585, 1998.

8. Colston, B. W., Jr., U. S. Sathyam, et al., "Dental OCT," *Optics Express*, Vol. 3, No. 6, 230–238, 1998.

9. Schmitt, J. M., "Optical coherence tomography (OCT): A review," *IEEE Journal of Selected Topics in Quantum Electronics*, Vol. 5, No. 4, 1205–1215, 1999.

10. Jones, R. S., G. D. Huynh, G. C. Jones, et al., "Near infrared transillumination at 1310 nm for the imaging of early dental decay," *Optics Express*, Vol. 11, No. 18, 2259–2265, 2003.

11. Fried, D., R. E. Glena, J. D. B. Featherstone, et al., "Nature of light scattering in dental enamel and dentin at visible and near-infrared wavelengths," *Applied Optics*, Vol. 34, No. 7, 1278–1285, 1995.

12. Yun, S. H., G. J. Tearney, J. F. Boer, et al., "High-speed optical frequency-domain imaging," *Optics Express*, Vol. 11, No. 22, 2953–2963, 2003.

13. Levoy, M., "Display of surfaces from volume data," *IEEE Computer Graphics and Application*, Vol. 8, No. 3, 29–37, 1988.

14. Elvins, T. T., "A survey of algorithms for volume visualization,"

Computer Graphics, Vol. 26, No. 3, 194–201, 1992.

15. Ray, H., H. Pfister, D. Silver, et al., "Ray casting architectures for volume," *IEEE Transactions on Visualization and Computer Graphics*, 1999.

16. Tang, Z. and J. Yuan, "Visualization of 3D data sets with image order volume rendering techniques," *Chinese J. Computers*, Vol. 17, No. 11, 801–808, 1994.

17. Levoy, M., "Efficient ray tracing of volume data," *ACM Transactions on Graphics*, Vol. 9, No. 3, 245–261, 1990.

18. Chen, Y., L. Otis, D. Piao, et al., "Characterization of dentin, enamel, and carious lesions by a polarization-sensitive optical coherence tomography system," *Applied Optics*, Vol. 44, No. 11, 2041–2048, 2005.

19. Jones, R. S., C. L. Darling, J. D. B. Featherstone, et al., "Imaging artificial caries on the occlusal surfaces with polarization-sensitive optical coherence tomography," *Caries Res.*, Vol. 40, 81–89, 2006.

20. Drexler, W. and J. G. Fujimoto, "State-of-the-art retinal optical coherence tomography," *Progress in Retinal and Eye Research*, Vol. 27, No. 1, 45–88, 2008.

21. Hayasaki, Y., "Holographic femtosecond laser processing and three-dimensional recording in biological tissues," *Progress In Electromagnetics Research Letters*, Vol. 2, 155–123, 2008.